iJRASET
International Journal For Research in Applied Science and Engineering Technology

# INTERNATIONAL JOURNAL FOR RESEARCH

IN APPLIED SCIENCE & ENGINEERING TECHNOLOGY

**Volume:** 12 **Issue:** VI **Month of publication:** June 2024

**DOI:** https://doi.org/10.22214/ijraset.2024.62599

www.ijraset.com

Call: 08813907089 | E-mail ID: ijraset@gmail.com

International Journal for Research in Applied Science & Engineering Technology (IJRASET)
*ISSN: 2321-9653; IC Value: 45.98; SJ Impact Factor: 7.538*
*Volume 12 Issue VI June 2024- Available at www.ijraset.com*

# Preparation and Characterization of $CuFeS_2$ Nanoparticles Synthesized via Hydrothermal Method

S. Vigneswaran[1,2], P. Gowthaman[1], S. Sangeethavanathi[1,2], M. Sathishkumar[3]
[1]*Department of Electronics, Erode Arts and Science College, Erode, India*
[2]*Department of Electronics, Sri Vasavi College, Erode, India*
[3]*Department of Electronics, Nehru Arts and Science College, Coimbatore, India*

***Abstract:** This research involved the successful synthesis of $CuFeS_2$ nanoparticles using a hydrothermal method. The $CuFeS_2$ nanoparticles were characterized using various analytical techniques, including X-ray diffraction (XRD), Raman spectroscopy, field emission scanning electron microscopy (FESEM), energy-dispersive X-ray spectroscopy (EDX), UV-Visible spectroscopy, and Brunauer-Emmett-Teller (BET) surface area analysis. The tetragonal crystalline structure was determined using X-ray diffraction (XRD) examination, indicating a particle size of 14 nm. The existence of chalcopyrite $CuFeS_2$ nanoparticles was established by the analysis of Raman spectra. The amorphous morphology was observed by FESEM imaging. The existence of Cu, Fe,and S elements was verified using EDX analysis, with no significant impurities observed. The UV-Visible investigation revealed a significant capacity for absorption within the wavelength region of 500-600 nm, accompanied by an energy band gap of 2.35 eV. The examination of BETsurface area revealed a surface area of 62 $m^2/g$ and a pore size of 10 nm. The obtained findings suggest that the $CuFeS_2$ nanoparticles possess favorable properties that render them appropriate for use in photocatalytic applications.*

***Keywords:** $CuFeS_2$, Chalcogenides, Hydrothermal Method, Characterization analysis.*

## I. INTRODUCTION

Nanomaterials have attracted considerable interest in recent years owing to their distinctive characteristics and possible uses in industries including electronics, catalysis, sensing, and environmental remediation [1-2]. Transition metal chalcogenides have garnered significant attention as potential nanomaterials due to their unique electrical, optical, and catalytic characteristics [3-5]. Chalcopyrite copper iron sulfide ($CuFeS_2$) is a semiconductor compound that belongs to the I-III-$VI_2$ ternary group. The material has distinctive characteristics, includinga high Neel temperature and outstanding electrical and optical capabilities, characterized by a very narrow optical band gap [6]. $CuFeS_2$ sometimes referred to as chalcopyrite, is a ternary compound that has intriguing properties such as a small bandgap, high absorption coefficient, and exceptional chemical stability. $CuFeS_2$ nanoparticles possess these characteristics that renderthem very appealing for use in solar cells, photocatalysis, and photovoltaic systems [7].

Nevertheless, the achievement of successful synthesis and comprehensive characterization of $CuFeS_2$ nanoparticles is crucial in order to fully harness their capabilities in many technological domains. Within this particular context, the hydrothermal approach emerges as a very adaptable and efficient methodology for the production of nanoparticles, exhibiting meticulous control overtheir dimensions, structure, and crystalline properties [8]. The characteristics of the resultant nanoparticles may be customized to match particular needs by manipulating reaction parameters, including temperature, pressure, and precursor concentrations. Several synthesis methods have been explored to fabricate $CuFeS_2$ nanoparticles, each offering distinct advantages and challenges. The synthesis method involves the controlled hydrothermal reaction of copper, iron, and sulfur precursors to generate nanoparticles that are uniform and well-defined. Among these methods, the hydrothermal synthesis route has gained significant attention for its ability to produce nanoparticles with controlled size, morphology, and crystallinity. The hydrothermal method involves the reaction of precursor materials under elevated temperature and pressure conditions in an aqueous solution, facilitating the nucleation and growth of $CuFeS_2$ nanoparticles with tailored properties [9-10].

Understanding the structural and optical properties of $CuFeS_2$ nanoparticles is crucial for optimizing their synthesis and harnessing their potential in various applications. The crystal structure of $CuFeS_2$, characterized by a tetragonal lattice arrangement, influences its electronic and optical behaviors [11].

 

Additionally, the bandgap of $CuFeS_2$ can be tuned by adjusting its composition and morphology, enabling tailored absorption properties for specific applications. The optical properties of $CuFeS_2$, including its absorption and emission spectra, play a pivotal role in applications such as photovoltaics, photocatalysis, and sensing. $CuFeS_2$ nanoparticles exhibit unique optical properties arising from quantum confinement effects and surface plasmon resonance phenomena, which can be exploited for efficient light harvesting and charge separation in photovoltaic devices, as well as for enhancing catalytic activity in photocatalytic reactions [12]. Furthermore, $CuFeS_2$ nanoparticles have garnered attention for their promising applications in various fields, including solar cells, photoelectrochemical devices, gas sensors, and biomedical imaging. The tunable bandgap and high absorption coefficients of $CuFeS_2$ make it an ideal candidate for photovoltaic applications, while its catalytic activity and biocompatibility render it suitable for sensing and biomedical applications [13].

In this study, we embark on a comprehensive exploration of $CuFeS_2$ nanoparticles fabricated through the hydrothermal method, delving into their production, analysis, and prospective applications. Through meticulous synthesis processes, we successfully generate $CuFeS_2$ nanoparticles, followed by an exhaustive evaluation employing a diverse array of analytical techniques. Our findings underscore the remarkable potential of these nanoparticles across various technological domains, with particular emphasis on their applicability in photocatalysis.

## II. EXPERIMENTAL SECTION

The hydrothermal method was employed for the facile synthesis of $CuFeS_2$ particles. Initially, copper chloride (1 mol; $CuCl_2$; Sigma–Aldrich) and ferric chloride (1 mol; $FeCl_36H_2O$; Sigma– Aldrich) were dissolved in 100 mL of pure water under continuous stirring for duration of 60 minutes. Following this, thiourea (1 mol, $(NH_2)_2CS$, Sigma–Aldrich) was gradually added to the CuFe solution, reaching a volume of 100 ml. The resulting $CuFeS_2$ solution was then transferred into a Teflon-lined stainless steel autoclave and maintained at a temperature of 180°C for a period of 12 hours. After the hydrothermal reaction, the obtained powders underwent filtration and were thoroughly washed with hot distilled water before undergoing vacuum drying. The residual substance was collected, washed with deionized water, and subsequently incubated overnight at 45°C to ensure complete drying. Additionally, a schematic representation of the experimental setup is provided in Figure 1.

The synthesized $CuFeS_2$ nanoparticles underwent comprehensive characterization utilizing state- of-the-art analytical techniques to elucidate their structural, morphological, elemental composition, surface area, and optical properties. Structural analysis was performed using a high-resolution X-ray diffractometer (XRD) (XPERT-PRO) to determine the crystalline structure, while Raman spectroscopy (WITech CRM200) provided insights into the molecular vibrational modes. Morphological and elemental composition analysis was carried out using a Field Emission Scanning Electron Microscope (FESEM) (Sigma HV – Carl ZEISS) equipped with Bruker Quantax 200-Z10 Energy-Dispersive X-ray Spectroscopy (EDS) detector. The surface area of the nanoparticles was determined using a Nova 2200e Analyzer through $N_2$ adsorption and desorption processes. Optical properties were investigated using UV-Vis spectrometer (Hitachi-UH5300, $\lambda$ = 200–900 nm) to assess their absorbance characteristics in the ultraviolet-visible range. These characterization techniques collectively provided a comprehensive understanding of the synthesized $CuFeS_2$ nanoparticles, paving the way for their potential applications in various technological fields.

## III. RESULTS AND DISCUSSION

Figure 2(A) presents the X-ray diffraction (XRD) analysis results of the synthesized $CuFeS_2$ nanoparticles. The diffraction pattern exhibits prominent peaks located at 2θ angles of 29.4º, 48.7º, and 59.7º, which correspond to the (112), (200), and (312) lattice planes, respectively. These peaks confirm the crystalline nature of the synthesized CuFeS2 nanoparticles, with the observed pattern closely matching the characteristic peaks of tetragonal chalcopyrite CuFeS2 as documented in the Joint Committee on Powder Diffraction Standards (JCPDS) card no. 37-0471. Notably, the peak at 29.4º corresponding to the (112) lattice plane exhibits the highest intensity, indicating its predominant presence in the synthesized $CuFeS_2$ nanoparticles. The Scherrer formula [14] was applied to estimate the crystallite size, revealing an average particle size of approximately 14 nm. This result underscores the influence of the hydrothermal method in enhancing the crystalline structure and controlling the particle size of $CuFeS_2$ nanoparticles. Based on the structural parameters obtained from XRD analysis (Table 1), the synthesized $CuFeS_2$ nanoparticles exhibit distinct features indicative of their crystalline nature and internal strain. The full width at half maximum (FWHM) values corresponding to the (112), (220), and

(312) lattice planes are 0.44328, 0.68822, and 1.03884 radians, respectively. These FWHM values reflect the degree of peak broadening, providing insights into the $CuFeS_2$ crystallite size distribution and internal strain within the nanoparticles.

Furthermore, the dislocation density (δ) and microstrain (ε) parameters offer valuable information about the structural defects and strain- induced distortions present in the synthesized $CuFeS_2$ nanoparticles. The observed microstrain values provide insights into the extent of lattice distortion and internal stress within the $CuFeS_2$ nanoparticles. Overall, the structural parameters obtained from XRD analysis elucidate the crystalline characteristics, internal strain, and defect density of the synthesized $CuFeS_2$ nanoparticles, contributing to a comprehensive understanding of their structural properties and potential applications.

The Raman spectrum of the synthesized $CuFeS_2$ sample is depicted in Figure 2(B), revealing several distinct peaks within the 100-700 $cm^{-1}$ range. Specifically, peaks are observed at wavenumbers of 151, 184, 323, 449, and 659 $cm^{-1}$. The presence of Cu-S bonds is indicated by peaks observed at 184 and 659 $cm^{-1}$, while the presence of Fe-S bonds is evidenced by the peak at 323 $cm^{-1}$. Additionally, a prominent peak corresponding to sulfur is observed at 183 $cm^{-1}$. The peak at 151 $cm^{-1}$ suggests the presence of S-S bonds. The dominant signal at 659 $cm^{-1}$ further confirms the presence of $CuFeS_2$ on the mineral surface of chalcopyrite. Chalcopyrite exhibits a complex stratified arrangement, with individual sulfur atoms within layers and sulfur dimers covalently bonded between layers. The observed Raman peaks provide insights into the molecular structure and bonding configuration of $CuFeS_2$, highlighting its unique characteristics and potential application [15-16].

Figure 2(C) presents the field emission scanning electron microscopy (FESEM) image of the synthesized $CuFeS_2$ sample. The FESEM imaging revealed an amorphous morphology, indicating the absence of well-defined crystalline structures. One possible reason for observing an amorphous morphology in synthesized $CuFeS_2$ nanoparticles via the hydrothermal method could be the rapid nucleation and growth kinetics under the specific reaction conditions employed. In the hydrothermal synthesis process, precursor materials are reacted in an aqueous solution under elevated temperature and pressure conditions, promoting the formation of nanoparticles through nucleation and subsequent growth [17]. Additionally, energy-dispersive X-ray spectroscopy (EDX) analysis was conducted to verify the elemental composition of the synthesized $CuFeS_2$ nanoparticles. Figure 2(D) shows the EDX spectrum, confirming the presence of copper (Cu), iron (Fe), and sulfur (S) elements in the sample. Importantly, no significant impurities were detected in the EDX analysis, underscoring the purity of the synthesized $CuFeS_2$ nanoparticles.

The UV-Visible absorbance spectra of the synthesized $CuFeS_2$, as depicted in Figure 3(A) within the wavelength range of 300-900 nm, revealed a distinct peak absorption observed prominently near 550 nm. This absorption behavior indicates the $CuFeS_2$ interaction with electromagnetic radiation in the visible region, suggestive of its potential optical applications. Further analysis involved the calculation of the $CuFeS_2$ band gap, achieved through the Tauc plot method illustrated in Figure 3(B), resulting in a determined value of 2.35 eV. The enhanced band gap observed in $CuFeS_2$ synthesized via the hydrothermal method can be attributed to several factors. The controlled growth conditions inherent to the hydrothermal synthesis process enable precise manipulation of reaction parameters, leading to the formation of materials with tailored electronic properties [18]. Additionally, this method facilitates the minimization of defects within the crystal lattice, ensures uniform particle size and distribution, and allows for better control over stoichiometry. Collectively, these factors contribute to the modification of the $CuFeS_2$ electronic band structure, ultimately resulting in the observed increase in the band gap, thus highlighting the efficacy of the hydrothermal method in tailoring the optical properties of $CuFeS_2$ for various applications

The surface area analysis of the synthesized $CuFeS_2$ nanoparticles, as depicted in Figure 3(C), involved examining the adsorption-desorption isotherms of nitrogen molecules to characterize the material's surface area and pore structure. The analysis revealed a significant surface area of 62 $m^2/g$ and a corresponding pore size of 10 nm, as illustrated in Figure 3(D). Notably, the nitrogen adsorption-desorption isotherm displayed type III behavior with hysteresis loops, indicating the presence of mesoporous characteristics within the $CuFeS_2$ structure. The improved surface area observed for $CuFeS_2$ synthesized via the hydrothermal method can be attributed to several factors inherent to this synthesis technique [19]. Hydrothermal synthesis provides a controlled environment conducive to the formation of well-defined crystalline structures with high surface area-to-volume ratios. Additionally, the precise control over reaction parameters such as temperature, pressure, and pH facilitates the creation of nanoparticles with uniform size and distribution, thereby enhancing the overall surface area. Furthermore, the mesoporous characteristics observed in the synthesized CuFeS2 nanoparticles suggest the presence of interconnected pores, which can contribute to the increased surface area. Overall, the hydrothermal method enables the synthesis of $CuFeS_2$ nanoparticles with improved surface area, making them promising candidates for various applications. Moreover, hydrothermal synthesis allows for precise control over reaction parameters, leading to the formation of nanoparticles with uniform size and distribution. Furthermore, the hydrothermal environment promotes the growth of crystalline structures with high surface area-to-volume ratios. These factors collectively contribute to the enhanced surface area of $CuFeS_2$ nanoparticles synthesized via the hydrothermal method, rendering them promising candidates for various applications, including catalysis, sensing, and energy [20].

## IV. CONCLUSION

In conclusion, the hydrothermally synthesized $CuFeS_2$ nanoparticles were characterized using XRD, Raman, FESEM, EDX, UV-Visible, and BET surface area analysis. XRD revealed the $CuFeS_2$ nanoparticles exhibits the tetragonal chalcopyrite $CuFeS_2$ structure and the average particle size was 14 nm, indicating that the hydrothermal process controls particle size. FESEM imaging showed an amorphous morphology of $CuFeS_2$, probably owing to fast nucleation and growth kinetics. Raman spectroscopy revealed its molecular structure and bonding arrangement. EDX examination showed $CuFeS_2$ nanoparticles elemental composition without contaminants. UV-Visible spectroscopy showed strong absorption and a band gap of 2.35 eV, increased by controlled growth conditions and hydrothermal defect reduction. Additionally, BET surface area study showed a mesoporous surface area of 62 $m^2/g$ due to regulated synthesis and linked pore development. These results show that the hydrothermal approach can tune $CuFeS_2$ nanoparticles structural and optical characteristics, making them suitable for catalysis, sensing, and energy conversion.

## REFERENCES

[1] Dan Niu, Yijun Liu, Qunhu Xue, Zhihong Wu, Cheng Yao, Xinyu Guo, Anwen Ren, Peng Li, Fabricating $FeS_2$ and $CuFeS_2$ microspheres embedded into biomass derived porous carbon with excellent microwave absorption, Materials Today Communications, Volume 38, 2024, 108100,

[2] Julia da Silveira Salla, Guilherme Luiz Dotto, Dachamir Hotza, Richard Landers, Katia da Boit Martinello, Edson Luiz Foletto, Enhanced catalytic performance of $CuFeS_2$ chalcogenide prepared by microwave-assisted route for photo-Fenton oxidation of emerging pollutant in water, Journal of Environmental Chemical Engineering, Volume 8,Issue 5, 2020, 104077.

[3] Nenguba Poloko, Gwiranai Danha, Tshepho Gaogane, Processing and characterization of chalcopyrite ($CuFeS_2$) sample from Botswana, Procedia Manufacturing, Volume 35,2019, Pages 488-493.

[4] Bhoomi S. Shah, Jolly B. Raval, Deepak Kumar, Sunil H. Chaki, M.P. Deshpande, A review on ternary $CuFeS_2$ compound: Fabrication strategies and applications, Journal of Alloys and Compounds, Volume 938, 2023, 168566.

[5] Yang-Wei Lin, Ting-Yu Lai, Yu-Shu Pan, Xuan-Wei Fang, Hsing-Yi Chen, Chen-Hao Yeh, Tsunghsueh Wu, Enhanced catalytic performance of $CuFeS_2$ chalcogenides for activation of persulfate towards decolorization and disinfection of pollutant in water, Materials Chemistry and Physics, Volume 301, 2023, 127564.

[6] Yasmin Vieira, Gabriel Severo de Carvalho, Jandira Leichtweis, Clóvia Marozzin Mistura, Edson Luiz Foletto, Asad Nawaz, Salim Manoharadas, Renato Zanella, Guilherme Luiz Dotto, $CuFeS_2$ /activated carbon heterostructure as a microwave- responsive catalyst for reductive and oxidative degradation of ibuprofen, ketoprofen, anddiclofenac, Chemical Engineering Journal, Volume 480, 2024, 148060.

[7] Sivakumar Bose, Sivaprakasam Radhakrishnan, Byoung-Suhk Kim, Hyun Wook Kang, Formulation of amorphous carbon embedded $CuFeS_2$ hybrids for the electrochemical detection of Quercetin, Materials Today Chemistry, Volume 26, 2022, 101228.

[8] Aleem Ansari, Rashmi A. Badhe, Dipak G. Babar, Shivram S. Garje, One pot solvothermal synthesis of bimetallic copper iron sulfide ($CuFeS_2$) and its use as electrodematerial in supercapacitor applications, Applied Surface Science Advances, Volume 9, 2022, 100231.

[9] Ubaid ur Rehman, Khalid Mahmood, Arslan Ashfaq, Adnan Ali, Sofia Tahir, Salma Ikram, Abdul Rehman, Kashaf ul Sahar, Waqas Ahmad, Nasir Amin, Enhanced thermoelectric performance of hydrothermally synthesized $CuFeS_2$ nanostructures by controlling the Cu/Fe ratio, Materials Chemistry and Physics, Volume 279, 2022, 125765.

[10] Changsheng Xu, Jie Wang, Kewei Wu, Guocui Xi, Xuebu Hu, Lei Qiu, $CuFeS_2$ anchored in ethylenediamine-modified reduced graphene oxide as an anode material for sodium ion batteries, Materials Letters, Volume 308, Part B, 2022, 131164.

[11] Junyi Huang, Yuanhao Zhou, Shimao Deng, Yangzi Shangguan, Ranhao Wang, Qiuyue Ge, Xuezhen Feng, Zhigang Yang, Yongfei Ji, Ting Fan, Baiyang Chen, Boqiang Li, Chunmiao Zheng, Xijun Hu, Hong Chen, Photo-assisted reductive cleavage and catalytic hydrolysis-mediated persulfate activation by mixed redox-couple-involved $CuFeS_2$ for efficient trichloroethylene oxidation in groundwater, Water Research, Volume 222, 2022, 118885.

[12] P. Rupa Ranjani, P.M. Anjana, R.B. Rakhi, Solvothermal synthesis of $CuFeS_2$ nanoflakes as a promising electrode material for supercapacitors, Journal of Energy Storage, Volume 33, 2021, 102063.

[13] M. Sathishkumar, M. Saroja, M. Venkatachalam, Influence of (Cu, Al) doping concentration on the structural, optical and antimicrobial activity of ZnS thin films prepared by Sol-Gel dip coating techniques, Optik, Volume 182, 2019, Pages 774-785.

[14] Yunhui Wang, Xue Li, Yiyong Zhang, Xinyi He, Jinbao Zhao, Ether based electrolyte improves the performance of $CuFeS_2$ spike-like nanorods as a novel anode for lithium storage, Electrochimica Acta, Volume 158, 2015, Pages 368-373.

[15] Erika Dutková, Zdenka Bujňáková, Jaroslav Kováč, Ivan Škorvánek, María Jesus Sayagués, Anna Zorkovská, Jaroslav Kováč, Peter Baláž, Mechanochemical synthesis, structural, magnetic, optical and electrooptical properties of $CuFeS_2$ nanoparticles, Advanced Powder Technology, Volume 29, Issue 8, 2018, Pages 1820-1826.

[16] M.X. Wang, L.S. Wang, G.H. Yue, X. Wang, P.X. Yan, D.L. Peng, Single crystal of $CuFeS_2$ nanowires synthesized through solventothermal process, Materials Chemistry and Physics, Volume 115, Issue 1, 2009, Pages 147-150.

[17] K.M. Deen, E. Asselin, On the use of a naturally-sourced $CuFeS_2$ mineral concentrate forenergy storage, Electrochimica Acta, Volume 297, 2019, Pages 1079-1093.

[18] C Boekema, A.M Krupski, M Varasteh, K Parvin, F van Til, F van der Woude, G.A Sawatzky, Cu and Fe valence states in $CuFeS_2$, Journal of Magnetism and Magnetic Materials, Volumes 272–276, Part 1, 2004, Pages 559-561.

[19] S.K. Pradhan, B. Ghosh, L.K. Samanta, Mechanosynthesis of nanocrystalline $CuFeS_2$ chalcopyrite, Physica E: Low-dimensional Systems and Nanostructures, Volume 33, Issue 1, 2006, Pages 144-146.

[20] Yu-Hsiang A. Wang, Ningzhong Bao, Arunava Gupta, Shape-controlled synthesis of semiconducting $CuFeS_2$ nanocrystals, Solid State Sciences, Volume 12, Issue 3, 2010, Pages 387-390,

[21] M. Sathishkumar, S. Geethalakshmi, Enhanced photocatalytic and antibacterial activity of Cu:SnO2 nanoparticles synthesized by microwave assisted method, Mater. Today: Proc. 20 (1) (2020) 54-63.
[22] S. Kannan, N.P. Subiramaniyam, M. Sathishkumar, Investigation on the structural, optical and photocatalytic degradation properties of Zns/Mn:Zns thin films under visible light irradiation, Mater. Today: Proc. 38 (2) (2021) 907-912.
[23] S. Kannan, N.P. Subiramaniyam, M. Sathishkumar, Effect of annealing temperature and Mn doping on the structural and optical properties of ZnS thin films for enhanced photocatalytic degradation under visible light irradiation, Inorg. Chem. Commun. 119 (2020) 108068.
[24] M. Sathishkumar, M. Saroja, M. Venkatachalam, P. Gowthaman, S. Kannan, A. Balamurugan, rGO encapsulated ZnSphotocatalysts for enhanced hydrogen evolution, Mater. Lett. 323 (2022) 132534.
[25] S.K. Mani, M. Saroja, M. Venkatachalam, T. Rajamanickam, Antimicrobial activity and photocatalytic degradation properties of zinc sulfide nanoparticles synthesized by using plant extracts, J. Nanostruct. 8 (2) (2018) 107-118.
[26] S. Kannan, NP. Subiramaniyam, M Sathishkumar, A novel green synthesis approach for improved photocatalytic activity and antibacterial properties of zinc sulfide nanoparticles using plant extract of Acalyphaindica and Tridaxprocumbens, J. Mater. Sci.: Mater. Electron. 31 (12) (2020) 9846-9859.
[27] M Sathishkumar, AT Rajamanickam, M Saroja, Characterization, antimicrobial activity and photocatalytic degradation properties of pure and biosynthesized zinc sulfide nanoparticles using plant extracts, J. Mater. Sci.: Mater. Electron. 29 (16) (2018) 14200- 14209.

Figure Caption

Figure 1 Schematic representation for synthesis of $CuFeS_2$ nanoparticles
Figure 2 Synthesized $CuFeS_2$ nanoparticles (A) XRD Analysis (B) Raman spectrum (C) FESEMimages (D) EDX spectrum
Figure 3 Synthesized $CuFeS^2$ nanoparticles (A) UV-Visible absorbance spectrum (B) Tauc Plot (C) $N_2$ adsorption/ desorption (D) Pore size

Table 1 Calculated structural parameters of the prepared $CuFeS_2$ nanoparticles

| ples | 2θ | (hkl) | D spacing | WHM Radian) | Lattice constants | | crystallite size (nm) | Average crystallite size (nm) | Dislocation Density(δ) | Microstrain (ε) |
|---|---|---|---|---|---|---|---|---|---|---|
| | | | | | Lattice a = b (Å) | Para meter c (Å) | | | | |
| $CuFeS_2$ | 29.4 | 112 | 3.0390 | 0.44328 | 5.289 | 10.42 | 19.3 | 14 | 0.000196 | 0.001882 |
| | 48.7 | 220 | 1.8700 | 0.68822 | | | 13.2 | | 0.000363 | 0.001694 |
| | 57.9 | 312 | 1.5926 | 1.03884 | | | 9.1 | | 0.000577 | 0.002092 |

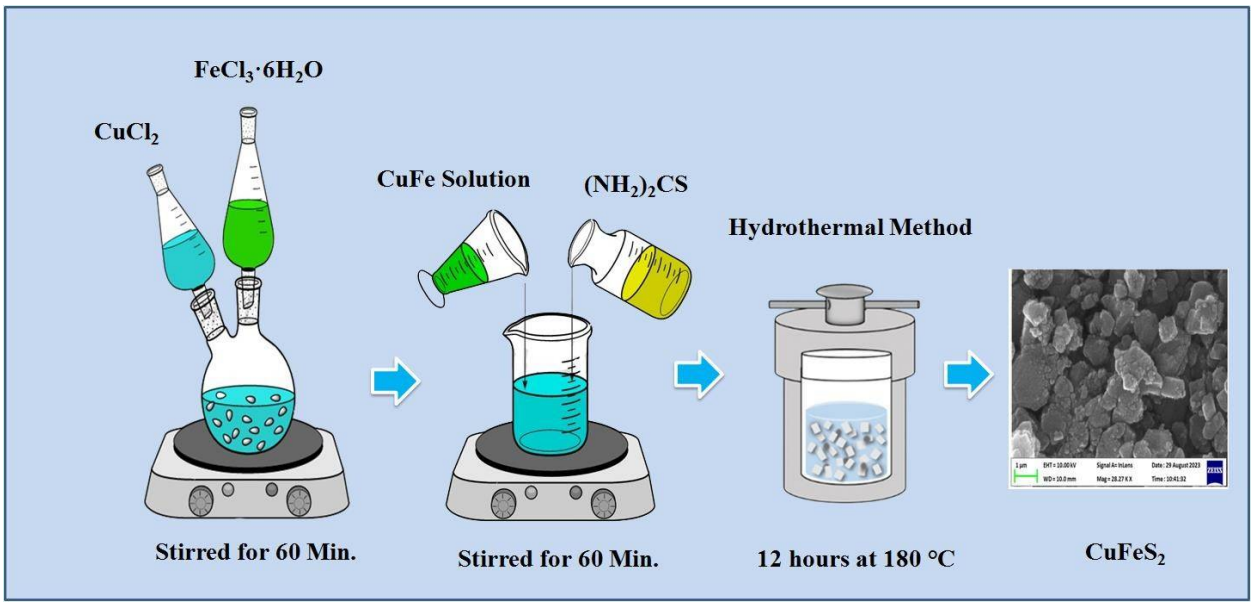


Figure 1 Schematic representation for synthesis of $CuFeS_2$ nanoparticles

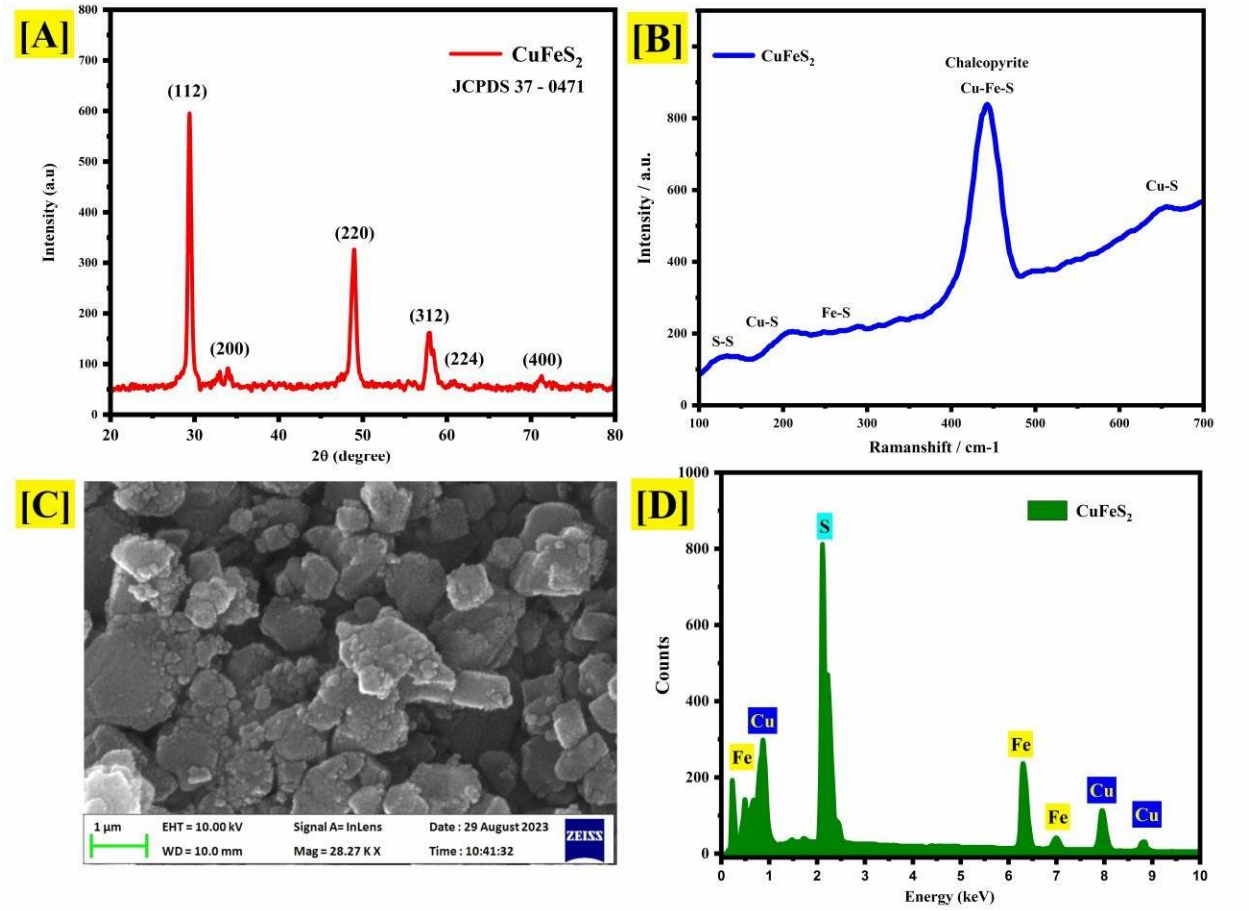


Figure 2 Synthesized $CuFeS_2$ nanoparticles (A) XRD Analysis (B) Raman spectrum (C) FESEM images (D) EDX spectrum

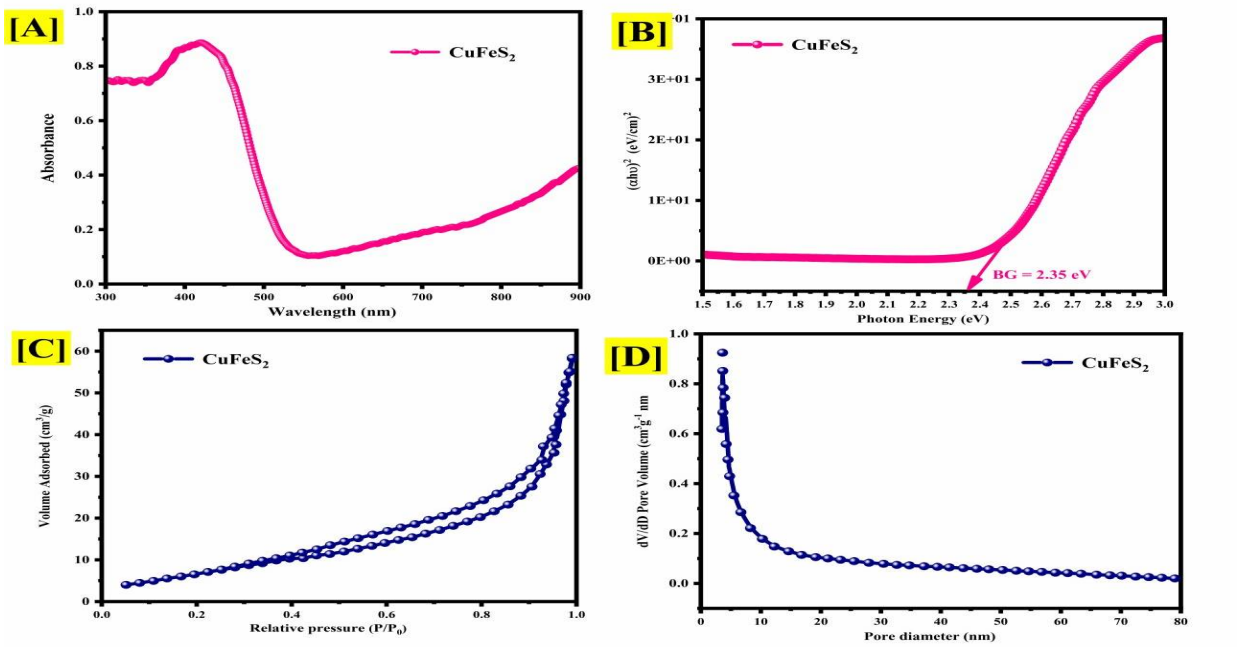


Figure 3 Synthesized $CuFeS_2$ nanoparticles (A) UV-Visible absorbance spectrum (B) Tauc Plot (C) $N_2$ adsorption/ desorption (D) Pore size

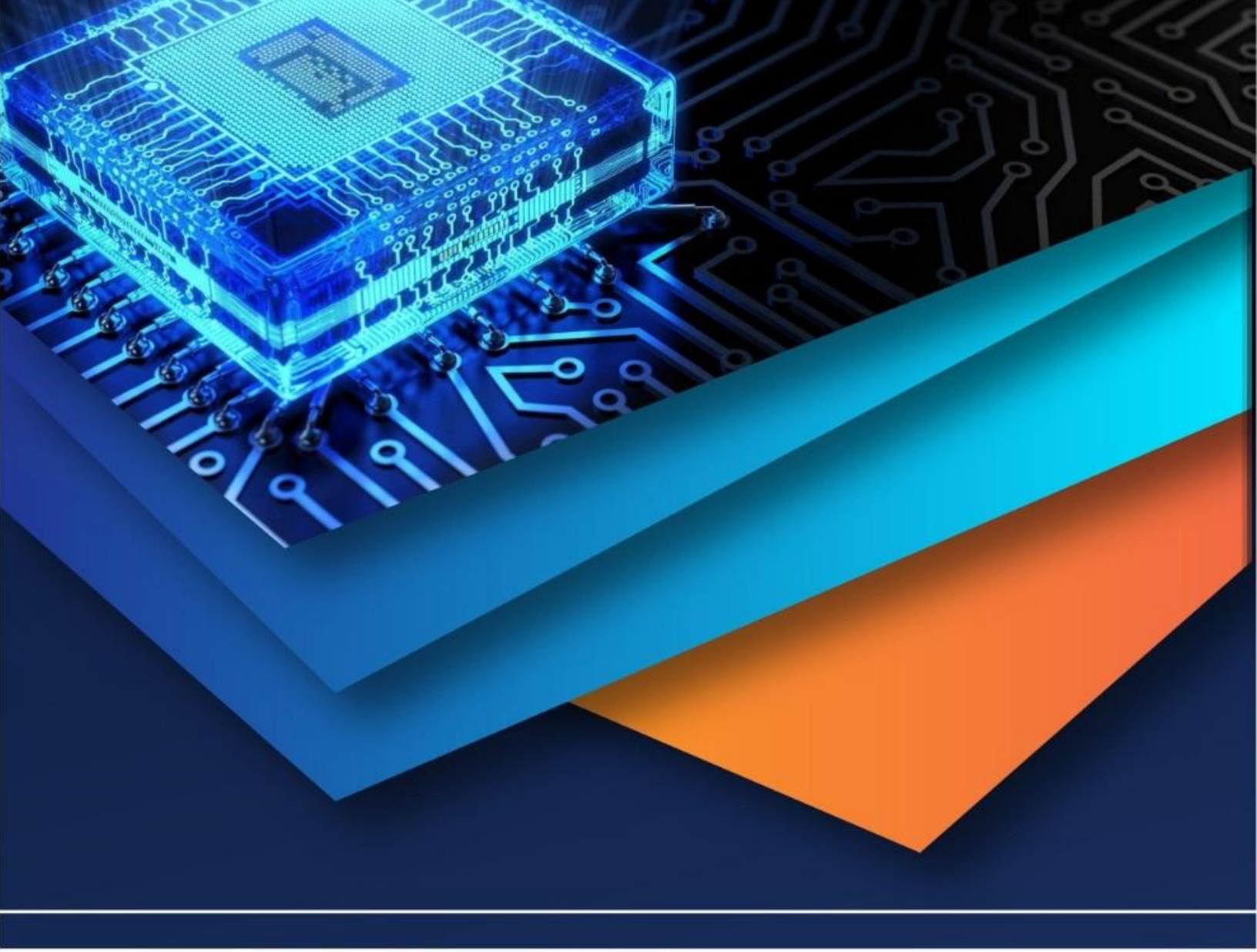

10.22214/IJRASET

45.98

IMPACT FACTOR: 7.129

IMPACT FACTOR: 7.429

# INTERNATIONAL JOURNAL FOR RESEARCH

IN APPLIED SCIENCE & ENGINEERING TECHNOLOGY